JGR Oceans

RESEARCH ARTICLE
10.1029/2022JC018897

The Influence of Sea Ice Cover and Atlantic Water Advection on Annual Particle Export North of Svalbard

C. Dybwad[1], C. Lalande[2], Y. V. Bodur[1], S. F. Henley[3], F. Cottier[1,4], E. A. Ershova[5,6], L. Hobbs[4,7], K. S. Last[4], A. M. Dąbrowska[8], and M. Reigstad[1]

[1]Department of Arctic and Marine Biology, UiT the Arctic University of Norway, Tromsø, Norway, [2]Amundsen Science, Université Laval, Québec, QC, Canada, [3]School of GeoSciences, University of Edinburgh, Edinburgh, UK, [4]Scottish Association for Marine Science, Oban, UK, [5]Institute of Marine Research, Bergen, Norway, [6]Shirshov Institute of Oceanology, Russian Academy of Sciences, Moscow, Russia, [7]Department of Mathematics and Statistics, University of Strathclyde, Glasgow, UK, [8]Marine Protists Laboratory, Department of Marine Ecology, Institute of Oceanology Polish Academy of Sciences, Sopot, Poland

Abstract The Arctic Ocean north of Svalbard has recently experienced large sea ice losses and the increasing prominence of Atlantic water (AW) advection. To investigate the impact of these ongoing changes on annual particle export, two moorings with sequential sediment traps were deployed in ice-free and seasonally ice-covered waters on the shelf north (NSv) and east (ESv) of Svalbard, collecting sinking particles nearly continuously from October 2017 to October 2018. Vertical export of particulate organic carbon (POC), total particulate matter (TPM), planktonic protists, chlorophyll *a*, and zooplankton fecal pellets were measured, and swimmers were quantified and identified. Combined with sensor data from the moorings, these time-series measurements provided a first assessment of the factors influencing particle export in this region of the Arctic Ocean. Higher annual TPM and POC fluxes at the ice-free NSv site were primarily driven by the advection of AW, higher grazing by large copepods, and a wind-induced mixing event during winter. Higher diatom fluxes were observed during spring in the presence of sea ice at the ESv site. Along with sea ice cover, regional differences in AW advection and the seasonal presence of grazers played a prominent role in the biological carbon pump along the continental shelf off Svalbard.

Plain Language Summary Recently, the area north of Svalbard has experienced the largest reduction of winter sea ice extent in the Arctic Ocean and an increasing influence of warm Atlantic water (AW) in surface waters. The consequences for the marine ecosystem remain unclear. In the present study, we investigated the fate of algal production and organic matter by measuring the amount and composition of the material sinking toward the seafloor. Using sediment traps with automatically rotating bottles, the seasonal variability in the quality and quantity of the organic matter sinking to ∼100 m was investigated at two sites with and without winter sea ice on the shelf north and east of Svalbard from 2017 to 2018. Our results suggest that the AW inflow along the shelf break induces a gradient with more zooplankton in the west and more ice in the east. More zooplankton in the west rework the organic matter through grazing, resulting in higher flux of carbon than in the east. Less zooplankton in the east potentially leaves more algal cells to sink ungrazed. As algal fluxes were higher in the presence of sea ice, a future with less sea ice may result in more reworked material sinking to the seafloor.

Key Points:

- Sea ice melt led to higher springtime and annual diatom fluxes at the seasonally ice-covered site
- Aside from algal fluxes, annual particle fluxes were higher at the ice-free site
- Atlantic water advection, zooplankton grazing, wind-induced mixing, and resuspension contributed to the higher fluxes at the ice-free site

Supporting Information:

Supporting Information may be found in the online version of this article.

Correspondence to:

C. Dybwad,
christine.dybwad@uit.no

Citation:

Dybwad, C., Lalande, C., Bodur, Y. V., Henley, S. F., Cottier, F., Ershova, E. A., et al. (2022). The influence of sea ice cover and Atlantic water advection on annual particle export north of Svalbard. *Journal of Geophysical Research: Oceans*, *127*, e2022JC018897. https://doi.org/10.1029/2022JC018897

Received 25 MAY 2022
Accepted 1 OCT 2022

Author Contributions:

Conceptualization: C. Dybwad, C. Lalande, Y. V. Bodur, M. Reigstad
Data curation: C. Dybwad
Formal analysis: C. Dybwad, C. Lalande, Y. V. Bodur, S. F. Henley, E. A. Ershova, A. M. Dąbrowska
Funding acquisition: F. Cottier, M. Reigstad
Investigation: S. F. Henley, F. Cottier, L. Hobbs, K. S. Last, M. Reigstad
Methodology: C. Dybwad, C. Lalande, Y. V. Bodur, F. Cottier, E. A. Ershova, M. Reigstad
Project Administration: F. Cottier
Resources: C. Dybwad, S. F. Henley, F. Cottier, M. Reigstad

1. Introduction

Across the Arctic Ocean, rapid sea ice retreat and thinning are occurring as a consequence of climate change (Stroeve & Notz, 2018). The Eurasian sector of the Arctic Ocean used to have prominent seasonal ice cover but has experienced large sea ice losses in recent years, especially during winter (Onarheim et al., 2018; Polyakov et al., 2017). The area north of Svalbard is part of the European Arctic Corridor with the greatest exchange of water in and out of the Arctic (Wassmann et al., 2010). The largest winter sea ice loss of the entire Arctic Ocean was recorded here between 1979 and 2012 (Onarheim et al., 2014), likely because of increased storm frequency and warmer temperatures of the Atlantic water (AW) advected into the area (Duarte et al., 2020; Renner et al., 2018). Unlike many regions of the Arctic Ocean that are strongly stratified, weakly stratified AW enters the area north and east of Svalbard and is exposed to direct ventilation in winter, caused by cooling and weakening of the halocline during sea-ice formation; a process called Atlantification (Polyakov et al., 2017). The shallower AW inflow

Software: C. Dybwad
Supervision: C. Lalande, Y. V. Bodur, M. Reigstad
Validation: C. Dybwad, C. Lalande, Y. V. Bodur, F. Cottier, M. Reigstad
Visualization: C. Dybwad, C. Lalande, Y. V. Bodur
Writing – original draft: C. Dybwad, C. Lalande, Y. V. Bodur, M. Reigstad
Writing – review & editing: C. Dybwad, C. Lalande, Y. V. Bodur, S. F. Henley, F. Cottier, E. A. Ershova, L. Hobbs, K. S. Last, A. M. Dąbrowska, M. Reigstad

brings advected heat and nutrients into the surface waters and is translating into ongoing ecosystem changes in the European Arctic corridor (Polyakov et al., 2020). Model estimates suggest greater inflow of nutrients and organic matter (Popova et al., 2013), phytoplankton biomass (Vernet et al., 2019), temperate phytoplankton species (Oziel et al., 2020), and Atlantic mesozooplankton (Wassmann et al., 2019). However, there is still a lack of in situ observations in this area to corroborate such estimates.

Winter sea ice loss is likely to have consequences for the marine ecosystem and the biological carbon pump along the continental slope off Svalbard. Sea ice controls the sunlight available for primary production and the stratification of the upper water column and supports ice algae growth and phytoplankton bloom development (Lalande et al., 2014; Leu et al., 2011). Algal bloom build-up and composition has direct consequences on the export of organic carbon to depth. Single-celled and chain-forming diatoms sink rapidly due to their silicified cell walls and are often associated with high export fluxes of carbon (Boyd & Newton, 1999; Dybwad et al., 2021), especially on termination of their growth phase (Agustí et al., 2020; Smetacek, 1985). By contrast, the small flagellate *Phaeocystis pouchetii* sinks slowly and contributes to lower carbon export efficiency (Reigstad & Wassmann, 2007; Wolf et al., 2016). Additionally, the timing between algal blooms and grazing by zooplankton influences the magnitude and composition of the organic matter exported to deeper waters and the seafloor. This will ultimately determine whether the exported carbon is dominated by ungrazed algae or fecal pellets (Wassmann, 1998; Wassmann et al., 2011).

Long-term measurements of vertical particle flux from the seasonally ice-covered Greenland Sea and the ice-free Norwegian Sea in the 1980s and 1990s suggest that annual carbon export is higher and under stronger zooplankton control in the Atlantic-influenced ice-free Norwegian Sea than in the cold Polar water-influenced Greenland Sea (von Bodungen et al., 1995). Particles fluxes obtained before, during, and after an anomalously warm AW inflow at the HAUSGARTEN observatory in the eastern Fram Strait indicated lower biogenic particulate silica (bPSi) fluxes (indicating diatoms) and smaller fecal pellets during the warm period, suggesting a community shift toward small-sized phytoplankton and zooplankton under warmer conditions (Lalande et al., 2013). However, bPSi and fecal pellet fluxes consistently increased in the presence of sea ice in the area, even during the warm anomaly, highlighting the key role of sea ice on export events (Lalande et al., 2013). Further observations in Fram Strait revealed higher carbon export of diatom-rich aggregates in ice-covered regions, compared to *P. pouchetii* aggregates in the ice-free region influenced by AW (Fadeev et al., 2021). In the main gateway for AW entering the Arctic Ocean, including the region north of Svalbard, where the presence of seasonal sea ice varies interannually and rapidly, long-term monitoring of vertical particle flux remains uninvestigated.

The current study aims to determine how spatial and seasonal variations in sea ice cover, ecosystem structure, and water properties influence particle flux and its composition on the shelf north of Svalbard. To achieve this goal, moored sediment traps were deployed at two sites with contrasting sea ice cover and water masses north and east of Svalbard from October 2017 to October 2018. The joint use of sediment traps and a suite of sensors allowed investigation of the magnitude, composition, and timing of downward particle fluxes in relation to sea ice cover, water properties, and biogeochemical parameters. The sensor data in the current study is an extension of that published by Henley et al. (2020). This study targets responses in an Arctic region where seasonal sea ice loss and AW influence is profound due to climate-driven changes in the cryosphere (Onarheim et al., 2014), where the productive season is extending (Kahru et al., 2016), and where an increasing influence of AW inflow on the physical and biogeochemical characteristics generates clear changes to the ecosystem (Ingvaldsen et al., 2021).

2. Methods

2.1. Mooring Sensors and Remote Sensing

Two moorings were deployed for two deployment cycles at a site ~70 km north of Svalbard (NSv) and at a site ~160 km east of Svalbard (ESv; Figure 1; Table 1). The moorings were deployed and/or recovered on board the RV *Lance* in September 2017, the RRS *James Clark Ross* in June 2018, and the RV *Kronprins Haakon* in November 2019. Each mooring was equipped with an SBE16Plus conductivity-temperature-depth (CTD) unit with WETLabs ECO fluorescence and LICOR biospherical photosynthetically active radiation (PAR) sensors deployed at ~25 m (Table 1). The PAR and fluorescence data were validated with the shipboard CTD-derived values obtained upon deployment and recovery of the moorings.

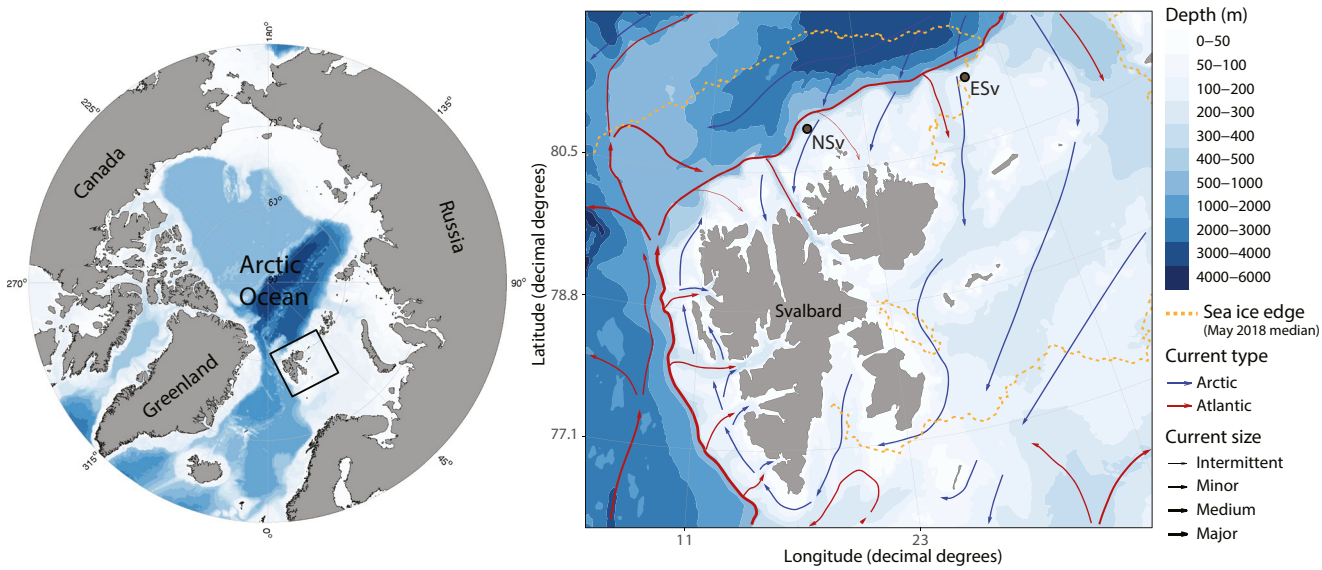

Figure 1. Mooring locations north (NSv) and east of Svalbard (ESv). Currents are indicated; the warm West Spitsbergen Current (Atlantic) and cold Arctic water. Median sea ice edge during May 2018 drawn from Meereisportal (AWI, Germany). The sediment traps were deployed at ~100 m with station depths ranging between 183 and 246 m (Table 1). Maps and currents are produced with the R package PlotSvalbard (Vihtakari, 2020).

In situ nitrate concentrations were measured at ~21 m using a SUNA V2 (submersible ultraviolet nitrate analyzer) with a biofouling wiper and processed following the methods detailed in Henley et al. (2020). Additionally, SBE37 CTD units and Star-Oddi temperature sensors were placed at intervals ranging between 4 and 25 m from top to bottom of the mooring, with a higher spatial resolution in the upper 100 m (Table 1). Water masses were differentiated using temperature, salinity, and density following water mass definitions according to Sundfjord et al. (2020).

Sea ice concentrations were extracted from satellite imagery using daily 3.125 km resolution Advanced Microwave Scanning Radiometer 2 data downloaded from http://seaice.uni-bremen.de/sea-ice-concentration/. The pixel closest to each mooring was used to extrapolate time-series of sea ice concentrations (0.58 km from the ESv mooring and 0.39 km from the NSv mooring) following Henley et al. (2020).

2.2. Sediment Traps

Sequential sediment traps (McLane Research Laboratories Inc., 21 bottles, aperture area of 0.5 m^2) were deployed at ~106 m on each mooring (Table 1). Sample bottles were programmed to rotate at intervals ranging from 7

Table 1
Mooring Deployment Information

Mooring	Latitude (°N)	Longitude (°E)	Sediment trap sampling period	Trap depth (m)	Water depth (m)	CTD depths (m)	Temperature sensor depths (m)
East of Svalbard (ESv)[a]	81°18.15	31°20.57	1 October 2017 to 2017 June 2018	106	183	24, 110, 171	31, 41, 51, 61, 83, 96, 125, 140, 155
	81°18.14	31°20.49	20 June 2018 to 2 August 2018	106	209	25, 36, 77, 111, 170	31, 36, 45, 55, 65, 83, 96, 125, 140, 155
North of Svalbard (NSv)[a]	81°02.03	18°24.80	1 October 2017 to 14 June 2018	107	234	22, 76, 111, 221	27, 31, 41, 51, 61, 96, 137, 187, 222
	81°02.04	18°24.84	22 June 2018 to 01 October 2018	107	246	28, 57, 78, 111, 222	33, 37, 47, 57, 67, 91, 97, 136, 161, 186

Note. East of Svalbard (ESv) = East Mooring (EM), north of Svalbard (NSv) = West Mooring (WM).
[a]Mooring names in Henley et al. (2020).

to 31 days, with more frequent rotation during spring and summer when higher fluxes were expected. Sample bottles were filled with filtered seawater poisoned with formalin (4% v/v), with the salinity adjusted to 40 by adding NaCl. No significant algal or animal growth was observed on the sediment traps upon recovery. As both moorings were recovered before the last rotation of the carousel in June 2018, the bottles that were open upon recovery were excluded from the analysis. During the second deployment period, the carousel failed to rotate past 16 August 2018 at ESv and 1 October 2018 at NSv.

2.3. Sample Analyses

First, each of the 500 ml samples were carefully homogenized and split into two 250 ml samples. From the original bottle, subsamples for chlorophyll *a* (chl *a*) measurements were taken to minimize light exposure, and subsamples (0.5–5 ml) were taken for the identification of planktonic protists and zooplankton fecal pellets. All zooplankton (swimmers) were carefully removed from one of the 250 ml subsamples for each sample using forceps. The swimmer-free subsamples were gently homogenized before subsamples (0.5–5 ml) were taken for total particulate matter (TPM), particulate organic matter (POM), particulate inorganic matter (PIM), particulate organic carbon (POC) and particulate nitrogen (PN). Subsamples for chl *a* were filtered onto GF/F Whatman filters (nominal pore size 0.7 μm, 25 mm diameter) that were placed in 100% methanol for 12 hr at 4°C–5°C in the dark to extract pigments. Chl *a* was measured using a pre-calibrated (Sigma, C6144) fluorometer (Turner Design AU-10).

Triplicate subsamples for TPM, POM, and PIM were filtered onto pre-combusted (7 hr at 450°C) and pre-weighed GF/F Whatman filters (pore size 0.7 μm). The filters were then rinsed with ultrapure Milli-Q water to remove salt, dried at 60°C overnight, and weighed using a microbalance to quantify TPM. The filters were then combusted for 7 hr at 450°C and weighed again on the microbalance to quantify PIM. By subtracting PIM from TPM, the amount of POM was determined. For the quantification of POC/PN, triplicate subsamples were filtered onto pre-combusted GF/F Whatman filters and frozen at −20°C until further analysis. The filters were dried at 60°C before being exposed to concentrated HCl fumes during 24 hr to remove inorganic carbon. The filters were dried again at 60°C for 24 hr before being packed into Nickel capsules and analyzed using a CHN elemental analyzer (Exeter Analytical CE440).

Subsamples (0.5–2 ml) for planktonic protists identification were settled in Utermöhl sedimentation chambers for 24 hr. Settled protists were counted using an inverted microscope equipped with phase and interference contrasts (Nikon Eclipse TE-300). Microplankton (>20 μm) was enumerated from the entire chamber surface at 100× magnification. Nanoplanktonic protists (3–20 μm) were counted at 400× magnification by moving the field of view along the length of three transverse transects (in special cases a magnification of 600× was used for taxonomic identification). The taxa were identified to the lowest taxonomic level possible following the World Register of Marine Species (WoRMS). Planktonic protist carbon (PPC) was calculated by multiplying the cell counts of individual cells and resting spores by the associated carbon content of each species or group depending on cell sizes (Menden-Deuer & Lessard, 2000), comparable to other studies in the area (Kubiszyn et al., 2014, 2017).

Zooplankton fecal pellets were enumerated using an inverted microscope (Zeiss Primovert) with length and width of each fecal pellet measured. The pellet volumes were calculated according to the shape of the pellets, with long cylindrical pellets attributed to copepods, larger fecal strings with cut ends (filiform) attributed to euphausiids (krill), and dense ellipsoid pellets attributed to appendicularians (larvaceans) and amphipods depending on their size and coloration (González, 2000; Riser et al., 2007). Fecal pellet volumes were converted into fecal pellet carbon (FPC) using a volumetric carbon conversion factor of 0.057 mg C mm^{-3} for cylindrical copepod pellets, 0.016 mg C mm^{-3} for cylindrical krill pellets, 0.042 mg C mm^{-3} for ellipsoid appendicularian pellets, and 0.038 mg C mm^{-3} for damaged and/or unidentified pellets (González et al., 1994).

Finally, 100–150 ml of the remaining samples were subsampled for the analysis of a minimum of 300 swimmers. Swimmers were identified to the lowest taxonomic level possible using a stereomicroscope (Zeiss Discovery V20) and measured with an accuracy of 10 μm using the ZoopBiom digitizing system (Roff & Hopcroft, 1986). The congeners *Calanus glacialis* and *Calanus finmarchicus* were separated from stage C4 and older based on size (Melle & Skjoldal, 1998). Biomass (dry weight) was estimated using published length-weight regressions for these or similar species (Ershova et al., 2015). The dry weight of each taxon was then converted to carbon

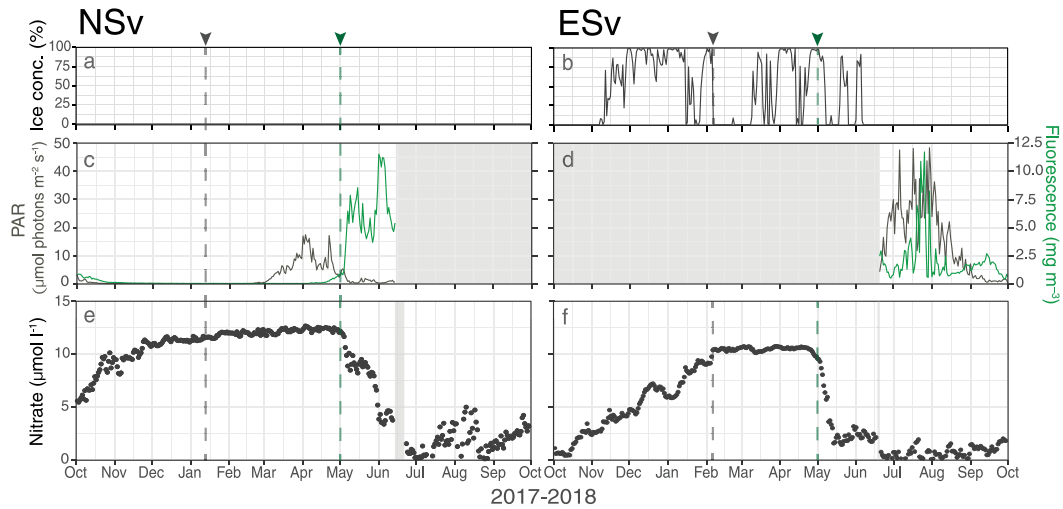

Figure 2. Sea ice concentration (a–b), photosynthetically active radiation (PAR) and fluorescence (c–d), and daily average nitrate concentrations (e–f) measured at ∼21 m at both mooring sites. Gray areas represent periods without data. Due to a malfunction of the SBE16 CTD unit during the first deployment cycle at ESv, the sensor was moved from the NSv to the ESv mooring for the second deployment. Gray dashed vertical lines represent water column mixing events and the green dashed vertical lines represent the initiation of a spring bloom inferred from a decrease in nitrate concentrations and/or increase in fluorescence.

weight following Kiørboe (2013). Species were also classified by biogeographic affinity (Table S1 in Supporting Information S1).

Daily fluxes were calculated depending on the volume of the subsamples, the trap area, and the sampling duration. Annual fluxes were integrated and extrapolated to 365 days.

3. Results

3.1. Sea Ice, Light, Fluorescence, and Nitrate

The region above the NSv site was ice-free throughout the study period (Figure 2a). By contrast, sea ice formed in early November 2017 at the ESv site and was sporadically present in large concentrations until June 2018, apart from a prolonged absence in February and March 2018 (Figure 2b).

Enhanced PAR values were recorded from early March–May 2018 at the NSv site, followed by a rapid increase in fluorescence in early May and a peak value of ∼11 mg m^{-3} recorded in early June 2018 (Figure 2c). At the ESv site, relatively high PAR and fluorescence values were observed in July and early August 2018, with fluorescence peaking at ∼11.5 mg m^{-3} (Figure 2d). While PAR values progressively decreased during August and September, fluorescence values were low until late September 2018.

At the NSv site, daily average nitrate concentrations steadily increased from ∼5 to 10 µmol l^{-1} from early October until December 2017, after which they remained >10 µmol l^{-1} until the following spring, with peak values reaching ∼12 µmol l^{-1} in late April 2018 (Figure 2e). By contrast, nitrate values were <1 µmol l^{-1} at the ESv site in October 2017, slowly increased during autumn and winter, and remained ∼10 µmol l^{-1} from February until early May 2018 (Figure 2f). Both mooring locations displayed rapid declines in nitrate concentrations in early May, with a faster decrease at ESv. Nitrate concentrations reached their lowest values (<1 µmol l^{-1}) in July 2018 at both sites. At the NSv site, nitrate concentrations varied in July and August before increasing to 4 µmol l^{-1} in late September 2018. At the ESv site, nitrate concentrations remained low during summer and increased to 2 µmol l^{-1} at the end of September 2018.

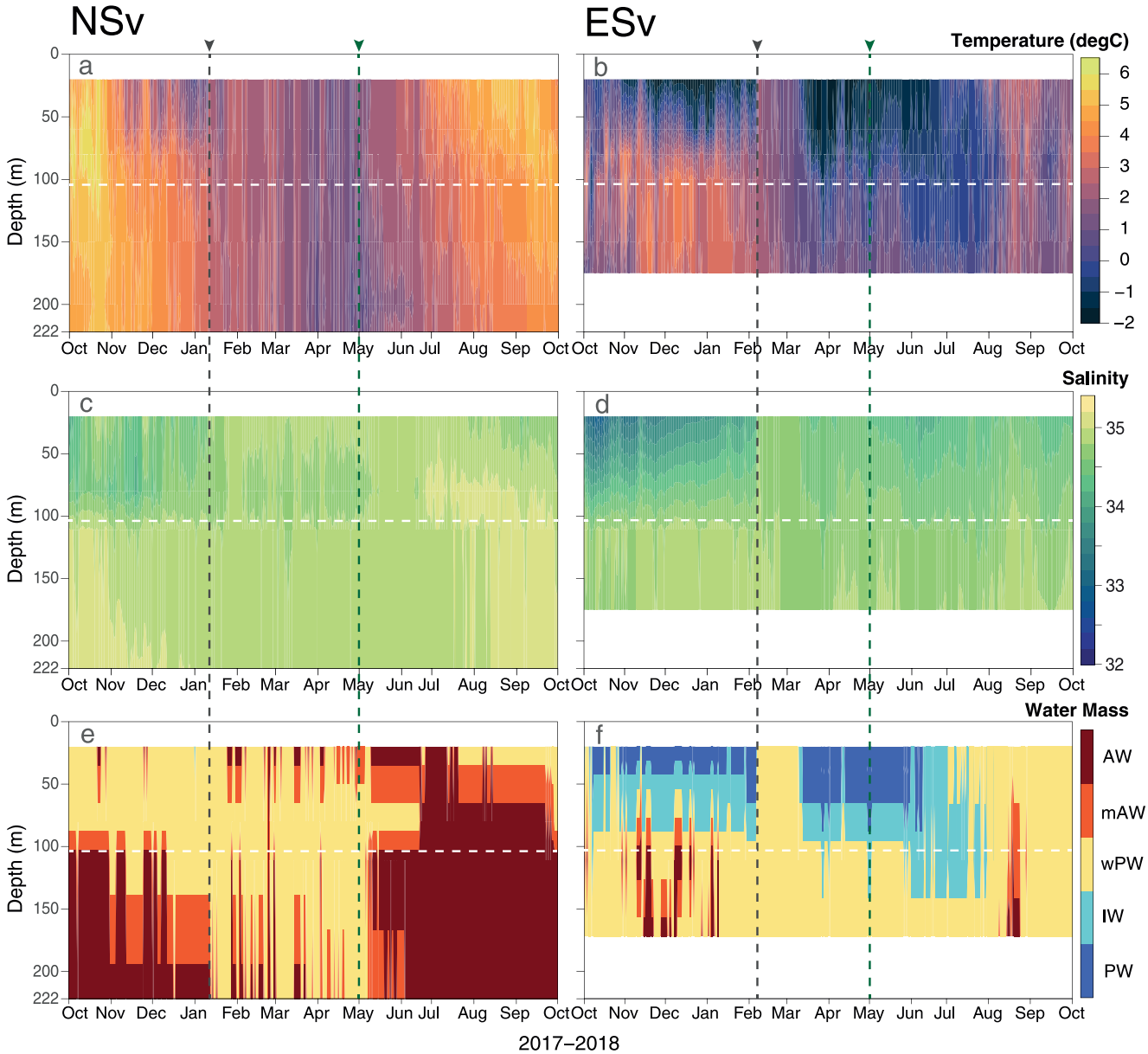

Figure 3. Average daily water temperature (a–b), salinity (c–d), and water masses (e–f) at both mooring sites. The water masses represent Atlantic Water (AW), modified Atlantic water (mAW), warm polar water (wPW), intermediate water (IW), and polar water (PW), following Sundfjord et al. (2020). Time-series of temperature and salinity at each site were made using linear interpolations between recorded depths. Nominal depths of the sensors were used as mooring tilt was minimal (<1.8 m of the upper-pressure sensor). Gray dashed vertical lines represent water column mixing events and the green dashed vertical lines represent the initiation of spring bloom. White dotted horizontal lines represent the depth of the sediment traps and white areas indicate depths outside sensor ranges.

3.2. Water Temperature and Salinity

At NSv, water temperatures at the trap depth (~100 m) generally decreased from 5.5°C to 0.5°C from October 2017 to May 2018 and increased back to 5°C from May–September 2018 (Figure 3a). Water temperature and salinity indicated the presence of a warm and more saline AW between 100 and 200 m from October–December 2017, with a layer of less saline warm polar water (wPW) observed from ~20 to 80 m during this period (Figures 3a, 3c and 3e). While wPW was prominent from January to May, AW again dominated a large proportion of the water column from May–September 2018 (Figure 3e).

By contrast, waters at the ESv site were colder and less saline than at the NSv site, with water temperatures <0°C from winter to late-summer between 20 and ~75 m, except for a period of more saline and warmer waters

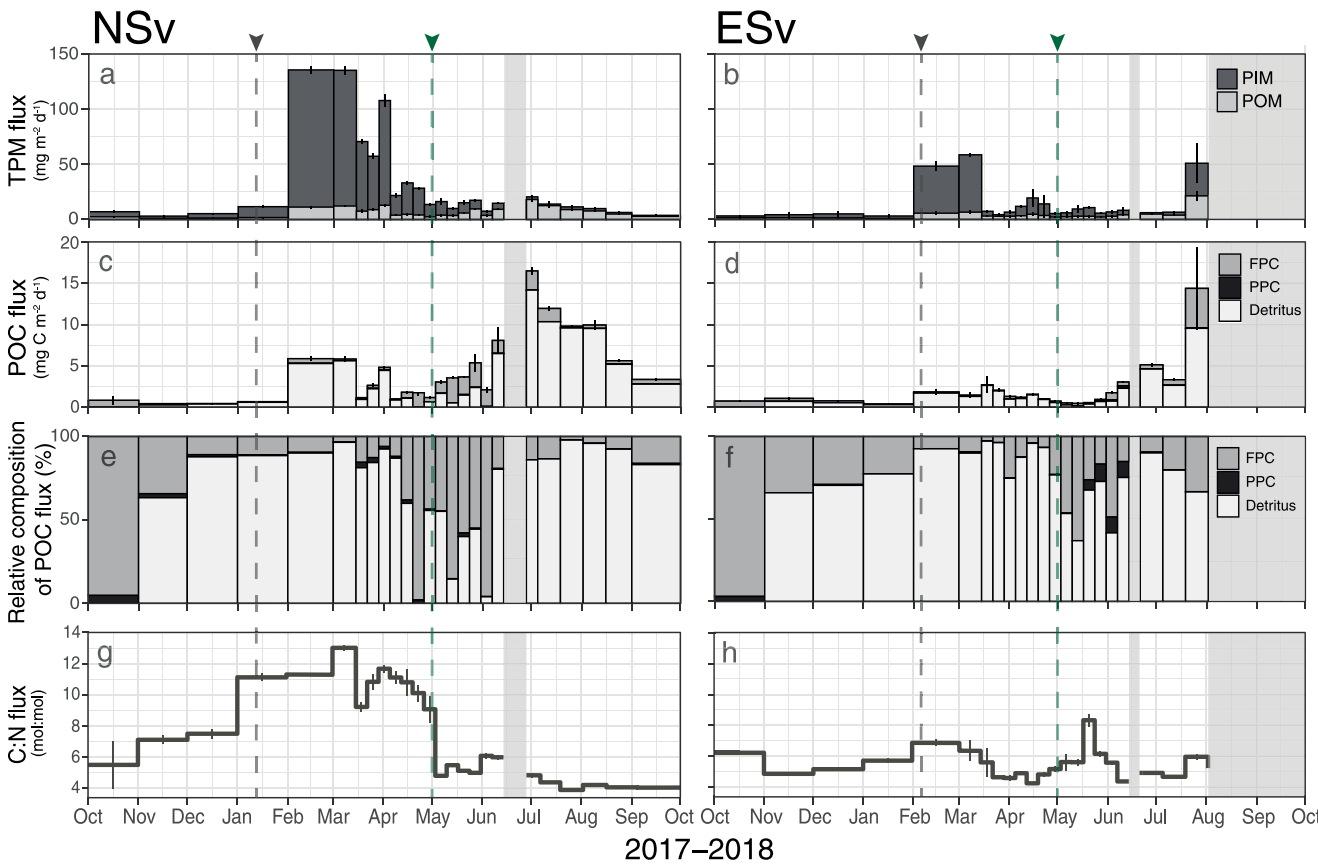

Figure 4. Total particulate matter (TPM) fluxes composed of particulate inorganic matter (PIM) and particulate organic matter (POM) (a–b), particulate organic carbon (POC) fluxes including compositional components of fecal pellet carbon (FPC), planktonic protist carbon (PPC) and remaining detritus (c–d), relative contribution of FPC, PPC and detritus to POC flux (e–f), and C:N ratios (g–h) at both mooring sites. Gray dashed vertical lines represent water column mixing events and the green dashed vertical lines represent the initiation of spring bloom. Gray areas indicate periods without data.

recorded in February–March 2018 (Figures 3b and 3d). Indeed, layers of cold polar water (PW) and intermediate water observed in the upper ~75 m of the water column from October 2017 to February 2018 were replaced from early February to early March by wPW recorded between 20 and 170 m (Figure 3f). Stratification was reestablished due to colder water from March to June 2018 (Figure 3f). Increased water temperatures from July to September 2018 coincided with the presence of wPW (Figures 3b–3f). While AW was sporadically present between ~100 and 170 m at ESv from November 2017 to January 2018 and during August 2018, AW was more present at the NSv site during autumn 2017 and summer 2018. Detailed information on stratification and wind stress at the mooring sites are available in Henley et al. (2020).

3.3. Total Particulate Matter and Particulate Organic Carbon Fluxes

At the NSv site, daily TPM fluxes were <30 mg m^{-2} d^{-1} except from February to early April 2018 when they increased to values ranging from 57 to 136 mg m^{-2} d^{-1}, representing a ~12-fold increase from January to February 2018 (Figure 4a, Table S2 in Supporting Information S1). At the ESv site, TPM fluxes increased above 45 mg m^{-2} d^{-1} during February, early March, and late July (Figure 4b). Most of the TPM exported (up to 92%) consisted of PIM, especially during winter (Figures 4a and 4b). POM fluxes consistently remained <25 mg m^{-2} d^{-1} at both sites. The highest POM fluxes (21 mg m^{-2} d^{-1}) were observed at ESv in late July 2018.

Roughly half of the POM fraction consisted of POC (Figures 4c and 4d). At NSv, daily POC fluxes >5 mg m^{-2} d^{-1} were observed during February and early March and from June–August 2018, with the highest POC flux of 16 mg m^{-2} d^{-1} recorded in late June-early July 2018 (Figure 4c). At ESv, POC fluxes >5 mg C m^{-2} d^{-1} were recorded in late June and late July 2018, with a peak POC flux of 14.4 mg C m^{-2} d^{-1} observed in late July

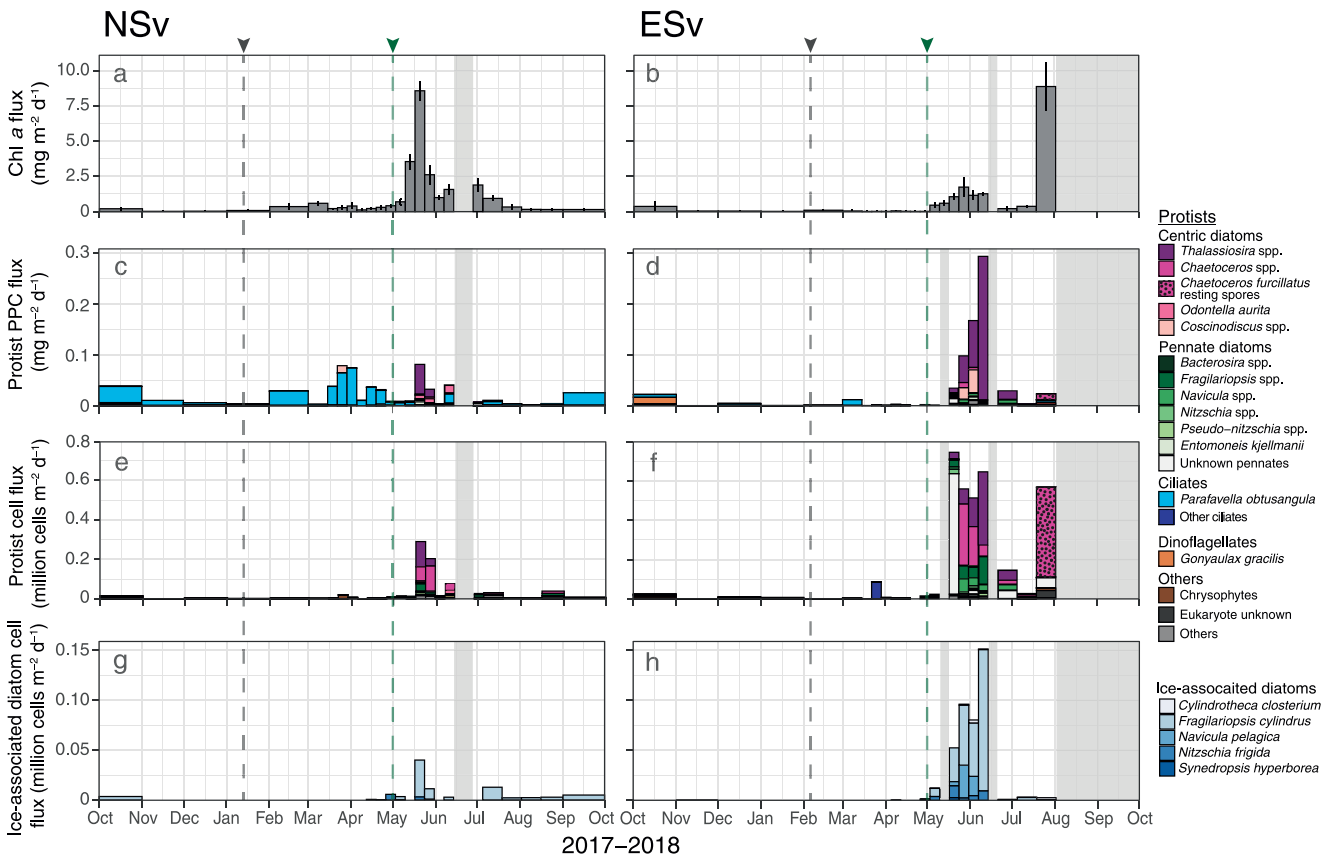

Figure 5. Chlorophyll a (chl a) (a–b), planktonic protist carbon (PPC) (c–d), protist cell (e–f), and ice-associated diatom cell fluxes (g–h) at both mooring sites. Gray dashed vertical lines represent water column mixing events and the green dashed vertical lines represent the initiation of spring bloom. Gray areas indicate missing data.

2018 (Figure 4d). The majority of POC exported at both sites was in the form of detritus or undiscernible POM (Figures 4c–4f). PPC contributions were generally very low, contributing to a slightly larger proportion of POC flux (10%) in late May and early June at the ESv site (Figure 4f). Enhanced FPC fluxes were observed during spring at NSv and during spring and late summer at ESv. During spring, FPC contributed up to 96% of the total POC flux at the NSv site (Figure 4e) and up to 63% at the ESv site (Figures 4e and 4f). Estimated FPC fluxes were larger than POC fluxes at both sites in October 2017 (213% and 168% at NSv and ESv, respectively; not shown).

C:N ratios (mol:mol) of the POM ranged between 4 and 8 from October to December 2017 and from May to September 2018 at NSv, as well as throughout the deployment period at ESv (Figures 4g and 4h). By contrast, higher C:N ratios ranging from 9 to 13 were observed from January to April 2018 at NSv (Figure 4h).

3.4. Chlorophyll *a* and Protist Fluxes

Chl *a* fluxes increased during spring and summer at both sites, with peak chl *a* fluxes observed during mid-May (8 mg m^{-2} d^{-1}) at NSv and during late July (9 mg m^{-2} d^{-1}) at ESv (Figures 5a and 5b).

PPC fluxes ranged between 0.003 and 0.04 mg C m^{-2} d^{-1} at the NSv site, with slightly higher fluxes during late March and late May (max 0.08 mg C m^{-2} d^{-1}; Figure 5c). Ciliates, mostly *Parafavella obtusangula*, dominated PPC fluxes most of the time, except in late May when centric diatoms *Thalassiosira* spp. contributed to the peak PPC fluxes (Figure 5c). The centric diatoms *Coscinodiscus* spp. and *Odontella aurita* significantly contributed to the diatom PPC fluxes at the NSv site in late March and June 2018, respectively. At ESv, PPC fluxes remained very low (mostly <0.01 mg C m^{-2} d^{-1}) except for a period of high diatom-associated PPC fluxes observed from late May to mid-June (max 0.29 mg C m^{-2} d^{-1}; Figure 5d). The dinoflagellate *Gonyaulax gracilis* dominated the PPC fluxes during October 2017, while the oligotrichid ciliate *P. obtusangula* contributed to the PPC fluxes in

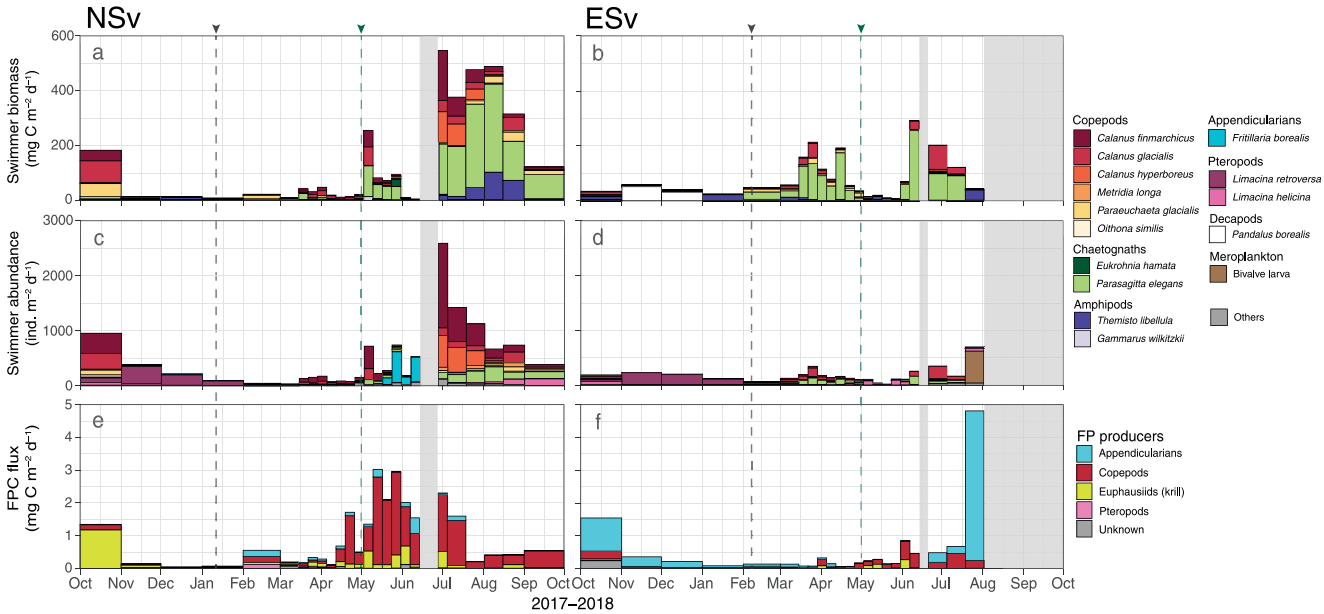

Figure 6. Dominant swimmer biomass (a–b), swimmer abundance (c–d), and fecal pellet carbon (FPC) fluxes (e–f) at both mooring sites. Gray dashed vertical lines represent water column mixing events and the green dashed vertical lines represent the initiation of spring bloom. Gray areas indicate missing data.

early March 2018 (Figure 5d). Note that the formalin solution was not buffered prior to deployment and small flagellate species may therefore have degraded in the samples.

Peak diatom cell fluxes were observed in late May at NSv and in May–June and late July at ESv (Figures 5e and 5f). While the centric diatoms *Thalassiosira* spp. contributed to most of the diatom PPC fluxes at both sites (Figures 5c and 5d), the centric diatoms *Chaetoceros* spp. made up large proportions of the cell fluxes during late May and early June at both sites (Figures 5e and 5f). In late July, a relatively high flux of resting spores of *Chaetoceros furcillatus* at ESv coincided with the largest chl *a* flux, but their small sizes translated into a minor contribution in terms of PPC flux (Figures 5d–5f). Pennate diatoms *Fragilariopsis* spp. and *Navicula* spp. also significantly contributed to the diatom fluxes during spring at the ESv site (Figure 5f). High diatom flux associated with unidentified pennate diatoms was observed in mid-May, but their small cell sizes did not result in increased PPC flux (Figures 5d–5f).

Very low fluxes of ice-associated diatoms, mostly of the pennate diatoms *Navicula pelagica* and *Fragilariopsis cylindrus* (Leu et al., 2015), were first observed in late April-early May at both sites and peaked in late May at the NSv site and in mid-June at the ESv site (Figures 5g and 5h). Although they were present and reached fluxes up to 150,000 cells m^{-2} d^{-1} during mid-June at ESv, their associated PPC flux accounted for <0.005 mg C m^{-2} d^{-1} during these periods.

3.5. Swimmers and Fecal Pellet Fluxes

At NSv, abundance and biomass of swimmers was largest during spring and summer (Figures 6a–6c). Despite the absence of a distinctive peak in swimmer abundance at ESv, swimmer biomass was also larger during spring and summer at that site (Figures 6b–6d). Copepods were constantly present at both sites, with a larger abundance collected at the NSv site (Figures 6c and 6d). Most of the copepods collected consisted of the small Atlantic *C. finmarchicus* at the NSv site and of the Arctic copepod *C. glacialis* at the ESv site. The large Arctic copepod *Calanus hyperboreus* was also periodically collected at NSv, especially in late June and July (Figure 6c). The large boreoarctic copepod *Paraeuchaeta glacialis* was sporadically observed at both sites, while low abundances of the small Arctic copepod *Oithona similis* were almost exclusive to NSv.

Chaetognaths, mostly the boreoarctic *Parasagitta elegans,* were present nearly continuously at both sites, except during winter (Figures 6a–6d). They contributed to most of the swimmer biomass during spring and summer at both sites due to their large size. The Arctic chaetognath *Eukrohnia hamata* was also present in small numbers

Table 2
Annual Vertical Fluxes at Both Mooring Sites

	Annual fluxes (mg m^{-2} yr^{-1}) [a]	
	NSv	ESv
Total particulate matter (TPM)	9,144	4,207
Particulate inorganic matter (PIM)	7,214	3,099
Particulate organic matter (POM)	1,924	1103
Particulate organic carbon (POC)	1,381	592
Fecal pellet carbon (FPC)	243	147
Planktonic protist carbon (PPC)	6	8
Chlorophyll *a* (chl *a*)	217	165
Protist cells	7	34

[a]Except protist cells (million cells m^{-2} yr^{-1}).

during summer at both sites. Despite low abundance, the boreoarctic amphipod *Themisto libellula* contributed to the swimmer biomass during summer at both sites and in January at the ESv site (Figures 6a and 6b). The small boreoarctic appendicularian *Fritillaria borealis* was abundant during spring at the NSv site, but not prominent in terms of biomass (Figure 6c).

The small Atlantic pteropod *Limacina retroversa* was collected at both sites from October to February, while the boreoarctic *Limacina helicina* was collected in May at ESv and late summer at NSv (Figures 6c and 6d). Bivalve larvae were abundant in late July at the ESv site (Figure 6d).

At the NSv site, enhanced FPC fluxes, mostly consisting of copepod fecal pellets, were observed from late April to mid-July 2018 (Figure 6e). At the ESv site, the highest FPC fluxes were observed during October 2017 and late July-early August 2018, when appendicularian pellets contributed to the majority of the FPC fluxes (Figure 6f). Relatively low copepod FPC fluxes were also observed from April to early August at the ESv site. Euphausiid FPC fluxes were larger and more frequent at the NSv site than at the ESv site (Figures 6e and 6f).

3.6. Annual Fluxes

Annual TPM fluxes were more than twice higher at the NSv site than at the ESv site (Table 2). The PIM contribution to TPM was slightly larger at the NSv site, making up ~79% of the annual flux compared to ~73% at the ESv site. Accordingly, the POM fraction represented ~21% of the TPM flux at the NSv site and ~26% at the ESv site. Annual POM fluxes had a ~72% contribution by POC at NSv and ~56% at ESv. Annual FPC and chl *a* fluxes were higher at the NSv site than at the ESv site, while annual PPC and protist cell fluxes were higher at ESv than NSv site. Annual FPC fluxes accounted for ~18% of the annual POC flux at the NSv site, and ~25% at the ESv site. Annual PPC flux accounted for ~0.4% of the annual POC flux at the NSv site, and ~1.4% at the ESv site. Annual protist cell fluxes were more than four times higher at the ESv site than at the NSv site.

4. Discussion

The nearly continuous monitoring of vertical fluxes from October 2017 to August or October 2018 at two sites north and east of Svalbard revealed spatial and seasonal variations in the timing, magnitude, and composition of vertical particle fluxes, reflecting the distinct influence of sea ice, warm AW, vertical mixing, and zooplankton grazing along the continental shelf.

4.1. Impact of Sea Ice Cover on Particle Flux

Annual TPM, POC, FPC, and chl *a* fluxes were higher at the ice-free NSv site, while annual PPC and protist cell fluxes were higher at the seasonally ice-covered ESv site. Although POC fluxes were generally low (<20 mg C m^{-2} d^{-1}) at both sites, the highest contribution of PPC to POC flux (~10%) was recorded during the spring bloom in May at the ESv site (Figure 4). PPC was mostly exported as pelagic diatoms *Thalassiosira* spp. and *Coscinodiscus* spp. (Figure 5). Diatoms are often associated with high export events in the Arctic Ocean as their ability to aggregate increases their sinking speed, especially under nutrient-limited conditions (Agustí et al., 2020; Roca-Martí et al., 2017; Smetacek, 1985). Previous studies in the Arctic seasonal ice zone where ice melt induces stratified conditions reported the build-up of large algal biomasses and high vertical POC and chl *a* fluxes (Andreassen & Wassmann, 1998; Dybwad et al., 2021; Wassmann & Reigstad, 2011). A recent study in the deep Fram Strait highlighted higher POC export including diatoms in the presence of sea ice than in regions without seasonal sea ice (Fadeev et al., 2021). As the presence of sea ice was not associated with larger POC fluxes during the spring bloom at ESv, other sources of POC are likely more important in the area north of Svalbard.

A rapid decline in nitrate concentrations and an increase in chl *a* and protist fluxes in early May at both sites resulted in the simultaneous onset of a spring bloom in the presence and absence of ice (Figure 5). Despite persistent sea ice cover in the beginning of May, small variations in daily sea ice concentrations or leads at the ESv site

during May likely facilitated sufficient irradiance in the upper water column. Sea ice melt in early May at the ESv site allowed for the stratification of the upper water column (Henley et al., 2020) and may have facilitated phytoplankton growth, supported by the rapid drawdown of nitrate recorded during the first 2 weeks of May (Figure 2). The highest diatom fluxes from mid-May to mid-June coincided with the depletion of nitrate concentrations. At the NSv site, the slower drawdown of nitrate (more than four times slower than at ESv [Henley et al., 2020]) may reflect a delay in stratification in the absence of melting sea ice, slowing down the build-up of a pelagic spring bloom (Behrenfeld, 2010; Reigstad et al., 2008; Sverdrup, 1953). In these conditions, grazing by zooplankton likely limited phytoplankton biomass, leading to lower protist cell fluxes and increased FPC fluxes at the NSv site. Similar observations have been reported for the North Atlantic and north of Svalbard (Wassmann, 2001).

The annual vertical PPC fluxes of 6 and 8 mg C m^{-2} yr^{-1} recorded at the NSv and ESv sites respectively were relatively low (Table 2). Higher annual PPC fluxes have been measured in the Eurasian Arctic Ocean (11–85 mg C m^{-2} yr^{-1}; Lalande et al., 2019) and in the Beaufort Sea (13–410 mg C m^{-2} yr^{-1}; Nadaï et al., 2021). The Eurasian Arctic Ocean sites often displayed large fluxes of the exclusively sympagic diatoms *Melosira arctica* and *Nitzschia frigida*, which sink fast and provide pulses of organic carbon to the seafloor (Bauerfeind et al., 1997; Boetius et al., 2013; Lalande et al., 2019). At the ESv site, the export of sympagic diatoms contributed to <0.2% of the vertical POC flux during the bloom at the end of May. Conversely, the PPC contributions of the exclusively pelagic diatoms *Thalassiosira* spp. and *Chaetoceros* spp. (16% and 70% at NSv and ESv, respectively) were often higher than in the Eurasian Arctic Ocean (Lalande et al., 2019). Despite low annual PPC fluxes and PPC contributions to annual POC fluxes of 0.4% and 1.4% north of Svalbard, contributions of PPC to annual POC fluxes rarely exceed 10% across the Arctic Ocean (Lalande et al., 2019; Nadaï et al., 2021).

Daily POC fluxes recorded at the ESv site were three times higher in late July (14 mg C m^{-2} d^{-1}) than during May following the spring bloom and contributed ~50% of the annual vertical POC flux. This summer export event consisted of algal cells with high chl *a* content, detritus and large appendicularian fecal pellets (Figures 4f and 6f). A simultaneous peak in fluorescence observed at 21 m recorded the sinking algae and source of food for appendicularians. As no coinciding nitrate drawdown was observed, some POC may have been advected into the area. Alternatively, this algal production could have been sustained by ammonium excreted by grazers, although there are no nutrient measurements available to support this hypothesis. The high chl *a* and diatom fluxes observed in late July were not associated with enhanced PPC flux due to the dominance of small *C. furcillatus* resting spores (Figure 5). These have low carbon content with a high cell area to volume ratio and are often observed in low nitrate concentrations when conditions are unfavorable for diatom growth (Chisholm, 1992). Conversely, *Chaetoceros* spp. resting spores have highly variable fluorescence and carbon content, contributing substantially to total vertical POC flux (9%–64%) in the sub-Arctic region of the Atlantic Ocean (Rynearson et al., 2013).

4.2. Impact of Winter Mixing on Particle Flux

Mixing events were observed in early January at the NSv site and in early February at the ESv site, coinciding with wind-stress events (Henley et al., 2020). At the ESv site, the wind-stress event pushed sea ice away from the mooring position starting on 6 February, led to warmer water temperature and higher salinity in the upper waters, and enhanced TPM fluxes during the ice-free period from February until mid-March (Figures 3 and 4). Despite experiencing the highest intensity of wind-induced mixing events (Henley et al., 2020), TPM fluxes were lower at the ESv site than at the NSv site. At the NSv site, a low-intensity but sustained wind stress event resulted in a well-mixed water column from January until May (Henley et al., 2020), while a prolonged period of high TPM fluxes was observed from February until April. Although current velocity data are unavailable for the 2017–2018 deployment period, increased current speeds of the AW advected into the area north of Svalbard were recorded during winter 2018–2019 (Koenig et al., 2022). A considerable and sustained disturbance of the seabed favoring resuspension is possible under sustained wind speeds promoting turbulence. Since the NSv site is situated closer to the AW core flowing along the shelf edge into the Arctic Ocean, mixing and resuspension may explain the enhanced TPM fluxes observed at this site.

High TPM and PIM fluxes along with enhanced POC fluxes in the absence of sunlight and primary production during winter at both sites further suggest input from resuspension events. This is supported by C:N ratios of sinking particles >11 at the NSv site during the mixing event (Figure 4g), similar to C:N ratios indicative of resuspended material observed during winter in the North Water polynya (Hargrave et al., 2002). The absence of notable increase in C:N ratios during the mixing event at the ESv site suggests that the organic fraction of the

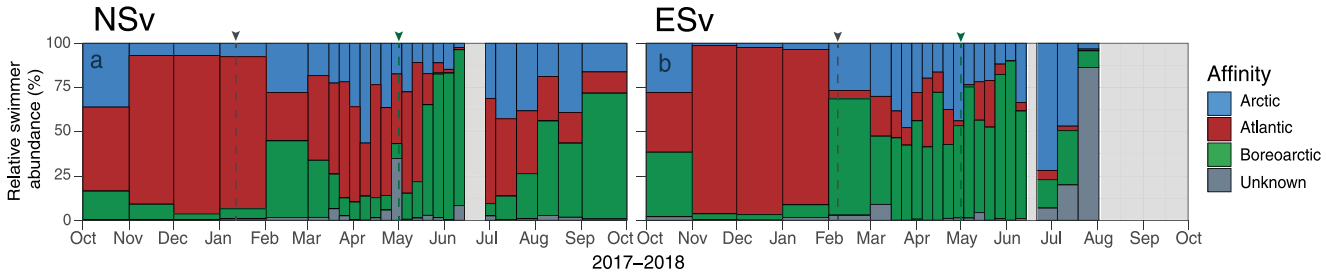

Figure 7. Biogeographical affinity of the swimmers collected at both mooring sites. Gray areas indicate missing data.

resuspended material was less degraded or of a different origin than at the NSv site. Nevertheless, these mixing events likely provided an important source of POC to the pelagic communities along the Svalbard continental slope during winter.

4.3. Impact of AW Advection on Particle Flux

The prominence of AW at the NSv site reflects its location in the Svalbard branch of the West Spitsbergen Current that transports warm AW into the Arctic Ocean. The AW core cools and is pushed deeper by PW as it moves further east along the continental slope (Figure 1; Cokelet et al., 2008; Menze et al., 2019). Accordingly, maximum winter nitrate values were higher at NSv, potentially contributing to the higher annual POC export. Elevated POC fluxes sustained in the presence of AW above the NSv sediment trap from mid-June to October 2018 support the advection of POC into the region.

A higher annual POC flux at the NSv site (1.4 g m^{-2} yr^{-1}) than at the ESv site (0.6 g m^{-2} yr^{-1}) also reflected the decreasing influence of AW along the shelf break. Slightly higher annual POC fluxes were measured in the eastern Fram Strait (1.5–2.5 g m^{-2} yr^{-1}; Bauerfeind et al., 2009; Lalande et al., 2016), while slightly lower annual POC fluxes were observed in the Amundsen Basin (0.5–0.6 g m^{-2} yr^{-1}) and Nansen Basin (0.6–0.8 g m^{-2} yr^{-1}; Lalande et al., 2019; Nöthig et al., 2020). The Fram Strait is strongly influenced by the inflow of AW at depth, contributing to slightly higher nutrients, phytoplankton biomass, and zooplankton biomass west of Svalbard than in the region north of Svalbard (Bluhm et al., 2015; Hirche & Kosobokova, 2007; Wassmann et al., 2015). By contrast, the Arctic Basins are strongly influenced by sea ice cover, leading to episodic and large vertical export events of ice algae (Boetius et al., 2013; Lalande et al., 2019). Therefore, particle fluxes obtained at the ice-free NSv site and seasonally ice-covered ESV site may reflect a transition zone between these two extremes in physical forcing. Further deployments of moorings with long-term sediment traps in these areas would be needed to validate this distinction.

POC fluxes in the absence and presence of sea ice at NSv and ESv were also reminiscent of POC fluxes obtained during a long-term monitoring study in the Norwegian Sea and the Greenland Sea where annual POC fluxes at 500 m ranged between 2.95 and 4.48 g C m^{-2} yr^{-1} in the ice-free Norwegian Sea and between 1.07 and 3.81 g C m^{-2} yr^{-1} in the seasonally ice-covered Greenland Sea (von Bodungen et al., 1995). Despite almost identical total annual primary productivity, the ice-free Norwegian Sea, where AW was prominent, was under stronger seasonal control of zooplankton grazing, combined with impact from lateral advection of resuspended material from the shelf regions. In the seasonally ice-covered Greenland Sea, dominated by water of polar origin, sea ice melt controlled early stratification, leading to the rapid onset of a diatom bloom and peak in particle fluxes.

A larger proportion of swimmers of Atlantic origin at the NSv site than the ESv site was also observed during spring and summer, dominated in biomass by the Atlantic copepod *C. finmarchicus* (Figure 7). Most of the *C. finmarchicus* individuals collected were copepodite stage V (CV) or adult females, with very few young copepodites and nauplii (data not shown). These results are in agreement with reports that *C. finmarchicus* is advected with AW and expatriated in the Arctic Ocean (Hirche & Kosobokova, 2007; Tarling et al., 2022). According to model estimates, the region of NSv experiences an annual influx of 22.3 g C m^{-2} yr^{-1} of *Calanus* spp. from AW advection, accounting for a biomass 12 times larger than produced locally (Wassmann et al., 2019). A significant contribution of advective biomass of large mesozooplankton was not observed at the ESv site (Figure 6d), in

agreement with decreasing abundance and biomass of *C. finmarchicus* from west to east along the AW inflow in the Arctic Ocean (Hirche & Kosobokova, 2007).

4.4. Impact of Zooplankton Grazing on Particle Flux

FPC fluxes reflect grazing activity and particle modification of importance for the biological carbon pump and energy flow through the food web (Wassmann, 1998). High FPC fluxes are frequently observed at high latitudes and upwelling areas of the world's oceans (Moigne, 2019). Annual FPC fluxes contributed to 18% and 24% of the annual POC fluxes at the NSv and ESv sites, respectively (Table 2). FPC fluxes and their contribution to POC fluxes were generally lowest during winter and highest during spring and autumn (Figures 6e and 6f), reflecting high grazing by larger zooplankton during the productive season and highlighting the role of fecal pellets in facilitating the rapid export of carbon from surface to depth (Turner, 2015). Similar vertical FPC fluxes to those observed at the NSv and ESv sites (2–5 mg C m^{-2} d^{-1}) have been reported in the Fram Strait (1–2 mg C m^{-2} d^{-1}, 15%–29% of POC flux; Lalande et al., 2013) and in deep waters over the Barents Sea continental slope (2–10 mg C m^{-2} d^{-1}, 10%–40% of POC flux; von Bodungen et al., 1995).

In general, FPC fluxes were higher at the NSv site than the ESv site (Figures 6e and 6f). At the NSv site, an increase in FPC fluxes coincided with the drawdown of nitrate and increase in fluorescence during May and early June, when FPC accounted for >50% of the POC exported. Specifically, elevated copepod FPC fluxes at that site suggest that large copepods such as *Calanus* spp. were present in large numbers and enforced a high grazing pressure at the initiation of the spring bloom. Zooplankton grazing pressure therefore likely contributed to the relatively low numbers of protist cells collected during the spring bloom at NSv (Figure 5). By contrast, very low FPC fluxes during the spring bloom at the ESv site coincided with higher diatom fluxes. While low diatom and high FPC fluxes at the NSv site indicated a match in the timing of algal production and zooplankton grazing, relatively high diatom and low FPC fluxes suggested a mismatch at the ESv site. This demonstrates that a match or mismatch in the timing of blooms and presence of grazing copepods will not only have an impact on the reproductive success of those grazers (Søreide et al., 2010), but also on the quantity and composition of the exported organic matter (Dezutter et al., 2019; Nadaï et al., 2021). A match between grazers and spring bloom previously observed in a nearby AW-influenced region north of Svalbard (Dybwad et al., 2021) further indicate the key role of AW inflow on the advection of zooplankton and the subsequent enhanced contribution of FPC in vertical POC fluxes.

Despite lower export of identifiable algal cells, chl *a* fluxes were higher during the spring bloom at NSv than at ESv (Figure 5). High FPC fluxes observed simultaneously to the elevated chl *a* fluxes potentially indicate the export of chl *a* as viable cells inside fecal pellets during the spring bloom (Jansen & Bathmann, 2007). Alternatively, this discrepancy may reflect the presence of algal cells that tend to somewhat degrade and are not easily visible with light microscopy in sequential sediment trap samples, such as the flagellate *Phaeocystis pouchetii*.

High appendicularian FPC fluxes were collected in October 2017 and late July 2018 at ESv (Figure 6). Appendicularian are filter-feeders that can respond rapidly to changes in food availability due to their high ingestion, growth, and reproduction rates (Hopcroft et al., 2005). They may have been able to respond quickly to the summer increase in algal biomass, reflected by increased fluorescence at 25 m and enhanced chl *a* and *C. furcillatus* resting spore fluxes in late July. Furthermore, the contribution of the large and rapidly sinking krill pellets (up to 862 m d^{-1}; Turner, 2015) was larger at the NSv site than at the ESv site. The highest krill FPC fluxes observed in October 2017 and during spring reflect their presence and grazing in the upper water column during these periods. Low krill FPC fluxes at the ESv site may be explained by their typically higher abundance in warmer AWs (Edwards et al., 2021; Riser et al., 2008; Zhukova et al., 2009). In the Barents Sea, they have been shown to feed at depth in AW when colder Arctic waters dominate surface waters (Riser et al., 2008). The collection of fecal pellets using long-term sediment traps reflects the presence and grazing activity of different zooplankton groups, including the presence and grazing activity of krill which has traditionally been difficult to constrain due to their patchy distribution and ability to avoid zooplankton nets (Nicol, 2003). Swimmers collected in the sediment traps also provide information on the seasonal development of the grazing community. *Calanus* spp. copepods were collected in large numbers at the end of June and in July at NSv (Figure 6c). This could indicate their entrapment during their downward seasonal migrations toward the end of the summer (Arashkevich et al., 2002) or during asynchronous migrations under the midnight sun when food was abundant in the upper water column (Cottier et al., 2006; Darnis et al., 2017). Either way, these migrations likely contributed to an active export fecal pellets

with high carbon content to depth (Wallace et al., 2013). The higher numbers of the chaetognath *P. elegans* during summer at NSv suggest that these tactile predators, whose main food source is copepods, follow their prey to deeper waters (Grigor et al., 2014).

As a fraction of swimmers may have been dead and passively sinking prior to entering the sediment trap, their inclusion as part of the flux may substantially increase the relatively low annual POC flux in the area north of Svalbard (Table 2). A study examining zooplankton communities north of Svalbard reported that up to 95% of *Calanus* spp. were dead in January (Daase et al., 2014). In the Canadian Arctic, roughly 5% of the swimmers collected in sediment traps were identified as dead passively sinking copepods, contributing to 36% of the annual vertical POC flux (Sampei et al., 2009). Hypothetically, if 5% of the annual swimmer biomass flux (Figures 6a and 6b) consisted of passively sinking carcasses, annual POC fluxes would increase to 3.6 g m^{-2} yr^{-1} (~260%) and 1.9 g m^{-2} yr^{-1} (~310%) at the NSv and ESv site, respectively. Disregarding dead swimmers may therefore seriously underestimate the annual downward POC flux. This potential additional contribution to annual POC flux could account for discrepancies in the carbon budget observed between vertical POC fluxes and benthic requirements (Wiedmann et al., 2020).

4.5. Conclusion and Perspectives

Continuous monitoring of particle fluxes indicated higher annual TPM and POC fluxes at the ice-free NSv site than at the seasonally ice-covered ESv site. However, higher annual protist flux at the ESv site suggests that seasonal ice melt induced the rapid stratification, onset and export of a spring diatom bloom at that site. By contrast, the AW-influenced NSv site displayed a slower stratification onset and a match between algal production and zooplankton grazers that led to higher POC export. These results indicate that particle fluxes in the area north of Svalbard are highly dependent on AW advection and therefore likely to increase with the ongoing Atlantification and continuous decline in sea ice due to global warming. In this context, the export of a diatom bloom at the onset of sea ice melt during spring may become less frequent, transitioning to an increasingly heterotrophic system with high recycling and vertical export of modified organic matter. Similar observations have been reported for the Fram Strait and along the West Spitzbergen Current (Dąbrowska et al., 2020; Fadeev et al., 2021). Finally, long-term biological, physical, and biogeochemical monitoring is fundamental to support and underpin reliable predictions on the impact of climate change on pelagic-benthic coupling in the future Arctic Ocean.

Data Availability Statement

All graphics and figures were made with R version 4.1.1 (R Core Team, 2021). The sequential sediment trap data are available via the NIRD Research Data Archive; https://doi.org/10.11582/2022.00044 for the particle flux data (Dybwad et al., 2022a), and https://doi.org/10.11582/2022.00045 for the protist and zooplankton flux data (Dybwad et al., 2022b). The data from the sensors on the moorings is available via the British Oceanographic Data Centre; https://doi.org/10.5285/e7db55e3-2899-1b40-e053-17d1a68b98b8 (Cottier et al., 2022a) for the NSv mooring and https://doi.org/10.5285/e7db55e3-2898-1b40-e053-17d1a68b98b8 (Cottier et al., 2022b) for the ESv mooring.

Acknowledgments
The authors are grateful to the Captains, Officers, Crews, and Science Teams onboard the RV Lance A-TWAIN Cruise in September 2017, the RRS James Clark Ross Cruise JR17006 in June 2018, and the Kronprins Haakon Cruise in November 2019. The authors thank Arild Sundfjord and UK National Marine Facilities for advice and technical support. The authors thank Lewis Drysdale, Luke Mardsen and Rahman Mankettikkara for their assistance in making the datasets available online. The authors thank the three anonymous reviewers for their useful suggestions. This work was jointly funded by UiT The Arctic University of Norway and Tromsø Research Foundation through the Arctic SIZE project (Arctic Seasonal Ice Zone Ecology, project number 01vm/h15), the Nansen Legacy project funded by the Research Council of Norway (project number 276730), and the Arctic PRIZE (PRoductivity in the seasonal Ice ZonE) project (Grant NE/P006302/1, NE/P006086/1) funded by the UK Natural Environment Research Council (NERC) Changing Arctic Ocean program.

References

Agustí, S., Krause, J. W., Marquez, I. A., Wassmann, P., Kristiansen, S., & Duarte, C. M. (2020). Arctic (Svalbard islands) active and exported diatom stocks and cell health status. *Biogeosciences*, *17*(1), 35–45. https://doi.org/10.5194/bg-17-35-2020

Andreassen, I. J., & Wassmann, P. (1998). Vertical flux of phytoplankton and particulate biogenic matter in the marginal ice zone of the Barents Sea in May 1993. *Marine Ecology Progress Series*, *170*, 1–14. https://doi.org/10.3354/meps170001

Arashkevich, E., Wassmann, P., Pasternak, A., & Riser, C. W. (2002). Seasonal and spatial changes in biomass, structure, and development progress of the zooplankton community in the Barents Sea. *Journal of Marine Systems*, *38*(1–2), 125–145. https://doi.org/10.1016/s0924-7963(02)00173-2

Bauerfeind, E., Garrity, C., Krumbholz, M., Ramseier, R. O., & Voβ, M. (1997). Seasonal variability of sediment trap collections in the Northeast Water Polynya. Part 2. Biochemical and microscopic composition of sedimenting matter. *Journal of Marine Systems*, *10*(1–4), 371–389. https://doi.org/10.1016/s0924-7963(96)00069-3

Bauerfeind, E., Nöthig, E.-M., Beszczynska, A., Fahl, K., Kaleschke, L., Kreker, K., et al. (2009). Particle sedimentation patterns in the eastern Fram Strait during 2000–2005: Results from the Arctic long-term observatory HAUSGARTEN. *Deep Sea Research Part I: Oceanographic Research Papers*, *56*(9), 1471–1487. https://doi.org/10.1016/j.dsr.2009.04.011

Behrenfeld, M. J. (2010). Abandoning Sverdrup's critical depth hypothesis on phytoplankton blooms. *Ecology*, *91*(4), 977–989. https://doi.org/10.1890/09-1207.1

Bluhm, B. A., Kosobokova, K. N., & Carmack, E. C. (2015). A tale of two basins: An integrated physical and biological perspective of the deep Arctic Ocean. *Progress in Oceanography*, *139*, 89–121. https://doi.org/10.1016/j.pocean.2015.07.011

Boetius, A., Albrecht, S., Bakker, K., Bienhold, C., Felden, J., Fernández-Méndez, M., et al. (2013). Export of algal biomass from the melting Arctic sea ice. *Science*, *339*(6126), 1430–1432. https://doi.org/10.1126/science.1231346

Boyd, P. W., & Newton, P. P. (1999). Does planktonic community structure determine downward particulate organic carbon flux in different oceanic provinces? *Deep Sea Research Part I: Oceanographic Research Papers*, *46*(1), 63–91. https://doi.org/10.1016/s0967-0637(98)00066-1

Chisholm, S. W. (1992). Primary productivity and biogeochemical cycles in the sea (pp. 213–237). https://doi.org/10.1007/978-1-4899-0762-2_12

Cokelet, E. D., Tervalon, N., & Bellingham, J. G. (2008). Hydrography of the West Spitsbergen Current, Svalbard branch: Autumn 2001. *Journal of Geophysical Research: Oceans (1978–2012)*, *113*(C1). https://doi.org/10.1029/2007jc004150

Cottier, F. R., Drysdale, L., Dumont, E., Henley, S. F., Hobbs, L., Porter, M., & Venables, E. (2022a). Arctic PRIZE western mooring data incorporating CTD, Nitrate, ADCP, and temperature sensors north of Svalbard at approximately 81°02'N, 18°25'E, September 2017 to November 2019 [Dataset]. NERC EDS British Oceanographic Data Center NOC. https://doi.org/10.5285/e7db55e3-2899-1b40-e053-17d1a68b98b8

Cottier, F. R., Drysdale, L., Dumont, E., Henley, S. F., Hobbs, L., Porter, M., & Venables, E. (2022b). Arctic PRIZE eastern mooring data incorporating CTD, Nitrate, ADCP, and temperature sensors, north of Svalbard at approximately 81°18'N, 31°20'E, September 2017 to November 2019 [Dataset]. NERC EDS British Oceanographic Data Center NOC. https://doi.org/10.5285/e7db55e3-2898-1b40-e053-17d1a68b98b8

Cottier, F. R., Tarling, G. A., Wold, A., & Falk-Petersen, S. (2006). Unsynchronized and synchronized vertical migration of zooplankton in a high Arctic fjord. *Limnology and Oceanography*, *51*(6), 2586–2599. https://doi.org/10.4319/lo.2006.51.6.2586

Daase, M., Varpe, Ø., & Falk-Petersen, S. (2014). Non-consumptive mortality in copepods: Occurrence of Calanus spp. carcasses in the Arctic Ocean during winter. *Journal of Plankton Research*, *36*(1), 129–144. https://doi.org/10.1093/plankt/fbt079

Dąbrowska, A. M., Wiktor, J. M., Merchel, M., & Wiktor, J. M. (2020). Planktonic protists of the eastern Nordic Seas and the Fram Strait: Spatial changes related to hydrography during early summer. *Frontiers in Marine Science*, *7*, 557. https://doi.org/10.3389/fmars.2020.00557

Darnis, G., Hobbs, L. J., Geoffroy, M., Grenvald, J. C., Renaud, P. E., Berge, J., et al. (2017). From polar night to midnight sun: Diel vertical migration, metabolism and biogeochemical role of zooplankton in a high Arctic fjord (Kongsfjorden, Svalbard). *Limnology and Oceanography*, *33*(1), 1719. https://doi.org/10.1002/lno.10519

Dezutter, T., Lalande, C., Dufresne, C., Darnis, G., & Fortier, L. (2019). Mismatch between microalgae and herbivorous copepods due to the record minimum sea ice extent of 2012 and the late sea ice break-up of 2013 in the Beaufort Sea. *Progress in Oceanography*. https://doi.org/10.1016/j.pocean.2019.02.008

Duarte, P., Sundfjord, A., Meyer, A., Hudson, S. R., Spreen, G., & Smedsrud, L. H. (2020). Warm Atlantic water explains observed sea ice melt rates north of Svalbard. *Journal of Geophysical Research: Oceans*, *125*(8). https://doi.org/10.1029/2019jc015662

Dybwad, C. S., Assmy, P., Olsen, L. M., Peeken, I., Nikolopoulos, A., Krumpen, T., et al. (2021). Carbon export in the seasonal sea ice zone north of Svalbard from winter to late summer. *Frontiers in Marine Science*, *7*, 3778–3821. https://doi.org/10.3389/fmars.2020.525800

Dybwad, C. S., Bodur, Y., Reigstad, M., & Cottier, F. (2022a). Nansen Legacy and Arctic PRIZE sequential sediment trap particle data, collected north of Svalbard from October 2017 to October 2018 [Dataset]. Norstore. https://doi.org/10.11582/2022.00044

Dybwad, C. S., Bodur, Y., Reigstad, M., & Cottier, F. (2022b). Nansen Legacy and Arctic PRIZE sequential sediment trap protist and zooplankton data, collected north of Svalbard from October 2017 to October 2018 [Dataset]. Norstore. https://doi.org/10.11582/2022.00045

Edwards, M., Hélaouët, P., Goberville, E., Lindley, A., Tarling, G. A., Burrows, M. T., & Atkinson, A. (2021). North Atlantic warming over six decades drives decreases in krill abundance with no associated range shift. *Communications Biology*, *4*(1), 644. https://doi.org/10.1038/s42003-021-02159-1

Ershova, E. A., Hopcroft, R. R., & Kosobokova, K. N. (2015). Interannual variability of summer mesozooplankton communities of the western Chukchi Sea: 2004–2012. *Polar Biology*, *38*(9), 1461–1481. https://doi.org/10.1007/s00300-015-1709-9

Fadeev, E., Rogge, A., Ramondenc, S., Nöthig, E.-M., Wekerle, C., Bienhold, C., et al. (2021). Sea ice presence is linked to higher carbon export and vertical microbial connectivity in the Eurasian Arctic Ocean. *Communications Biology*, *4*(1), 1255. https://doi.org/10.1038/s42003-021-02776-w

González, H. E. (2000). The role of fecal material in the particulate organic carbon flux in the northern Humboldt Current, Chile (23°S), before and during the 1997–1998 El Nino. *Journal of Plankton Research*, *22*(3), 499–529. https://doi.org/10.1093/plankt/22.3.499

González, H. E., Gonzalez, S., & Brummer, G.-J. (1994). Short-term sedimentation pattern of zooplankton, feces and microplankton at a permanent station in the Bjornafjorden (Norway) during April–May 1992. *Marine Ecology Progress Series*, *105*, 31–45. https://doi.org/10.3354/meps105031

Grigor, J., Søreide, J., & Varpe, Ø. (2014). Seasonal ecology and life-history strategy of the high-latitude predatory zooplankter Parasagitta elegans. *Marine Ecology Progress Series*, *499*, 77–88. https://doi.org/10.3354/meps10676

Hargrave, B. T., Walsh, I. D., & Murray, D. W. (2002). Seasonal and spatial patterns in mass and organic matter sedimentation in the North Water. *Deep Sea Research Part II: Topical Studies in Oceanography*, *49*(22–23), 5227–5244. https://doi.org/10.1016/s0967-0645(02)00187-x

Henley, S. F., Porter, M., Hobbs, L., Braun, J., Guillaume-Castel, R., Venables, E. J., et al. (2020). Nitrate supply and uptake in the Atlantic Arctic sea ice zone: Seasonal cycle, mechanisms, and drivers. *Philosophical Transactions of the Royal Society A*, *378*(2181), 20190361. https://doi.org/10.1098/rsta.2019.0361

Hirche, H.-J., & Kosobokova, K. (2007). Distribution of *Calanus finmarchicus* in the northern North Atlantic and Arctic Ocean—Expatriation and potential colonization. *Deep Sea Research Part II: Topical Studies in Oceanography*, *54*(23–26), 2729–2747. https://doi.org/10.1016/j.dsr2.2007.08.006

Hopcroft, R. R., Clarke, C., Nelson, R. J., & Raskoff, K. A. (2005). Zooplankton communities of the Arctic's Canada Basin: The contribution by smaller taxa. *Polar Biology*, *28*(3), 198–206. https://doi.org/10.1007/s00300-004-0680-7

Ingvaldsen, R. B., Assmann, K. M., Primicerio, R., Fossheim, M., Polyakov, I. V., & Dolgov, A. V. (2021). Physical manifestations and ecological implications of Arctic Atlantification. *Nature Reviews Earth and Environment*, 1–16. https://doi.org/10.1038/s43017-021-00228-x

Jansen, S., & Bathmann, U. (2007). Algae viability within copepod fecal pellets: Evidence from microscopic examinations. *Marine Ecology Progress Series*, *337*, 145–153. https://doi.org/10.3354/meps337145

Kahru, M., Lee, Z., Mitchell, B. G., & Nevison, C. D. (2016). Effects of sea ice cover on satellite-detected primary production in the Arctic Ocean. *Biology Letters*, *12*(11), 20160223. https://doi.org/10.1098/rsbl.2016.0223

Kiørboe, T. (2013). Zooplankton body composition. *Limnology and Oceanography*, *58*(5), 1843–1850. https://doi.org/10.4319/lo.2013.58.5.1843

Koenig, Z., Kalhagen, K., Kolås, E., Fer, I., Nilsen, F., & Cottier, F. (2022). Atlantic water properties, transport and heat loss from mooring observations north of Svalbard. *Journal of Geophysical Research: Oceans*, *127*(8). https://doi.org/10.1029/2022jc018568

Kubiszyn, A. M., Piwosz, K., & Wiktor, J. M. (2014). The effect of interannual Atlantic water inflow variability on the planktonic protist community structure in the West Spitsbergen waters during the summer. *Journal of Plankton Research*, *36*(5), 1190–1203. https://doi.org/10.1093/plankt/fbu044

Kubiszyn, A. M., Wiktor, J. M., Wiktor, J. M., Jr., Griffiths, C., Kristiansen, S., & Gabrielsen, T. M. (2017). The annual planktonic protist community structure in an ice-free high Arctic fjord (Adventfjorden, West Spitsbergen). *Journal of Marine Systems*, *169*, 61–72. https://doi.org/10.1016/j.jmarsys.2017.01.013

Lalande, C., Bauerfeind, E., Nöthig, E.-M., & Beszczynska-Möller, A. (2013). Impact of a warm anomaly on export fluxes of biogenic matter in the eastern Fram Strait. *Progress in Oceanography*, *109*, 70–77. https://doi.org/10.1016/j.pocean.2012.09.006

Lalande, C., Moriceau, B., Leynaert, A., & Morata, N. (2016). Spatial and temporal variability in export fluxes of biogenic matter in Kongsfjorden. *Polar Biology*, *39*(10), 1725–1738. https://doi.org/10.1007/s00300-016-1903-4

Lalande, C., Nöthig, E.-M., & Fortier, L. (2019). Algal export in the Arctic Ocean in times of global warming. *Geophysical Research Letters*, *46*(11), 5959–5967. https://doi.org/10.1029/2019gl083167

Lalande, C., Nöthig, E. M., Somavilla, R., Bauerfeind, E., Shevchenko, V., & Okolodkov, Y. (2014). Variability in under-ice export fluxes of biogenic matter in the Arctic Ocean. *Global Biogeochemical Cycles*. https://doi.org/10.1002/2013gb004735

Leu, E., Mundy, C. J., Assmy, P., Campbell, K., Gabrielsen, T. M., Gosselin, M., et al. (2015). Arctic spring awakening—Steering principles behind the phenology of vernal ice algal blooms. *Progress in Oceanography*, *139*, 151–170. https://doi.org/10.1016/j.pocean.2015.07.012

Leu, E., Søreide, J. E., Hessen, D. O., Falk-Petersen, S., & Berge, J. (2011). Consequences of changing sea-ice cover for primary and secondary producers in the European Arctic shelf seas: Timing, quantity, and quality. *Progress in Oceanography*, *90*(1–4), 18–32. https://doi.org/10.1016/j.pocean.2011.02.004

Melle, W., & Skjoldal, H. (1998). Reproduction and development of *Calanus finmarchicus*, *C. glacialis* and *C. hyperboreus* in the Barents Sea. *Marine Ecology Progress Series*, *169*, 211–228. https://doi.org/10.3354/meps169211

Menden-Deuer, S., & Lessard, E. J. (2000). Carbon to volume relationships for dinoflagellates, diatoms, and other protist plankton. *Limnology and Oceanography*, *45*(3), 569–579. https://doi.org/10.4319/lo.2000.45.3.0569

Menze, S., Ingvaldsen, R. B., Haugan, P., Fer, I., Sundfjord, A., Moeller, A. B., & Petersen, S. F. (2019). Atlantic water pathways along the north-western Svalbard shelf mapped using vessel-mounted current profilers. *Journal of Geophysical Research: Oceans*, *124*(3), 1699–1716. https://doi.org/10.1029/2018jc014299

Moigne, F. A. C. L. (2019). Pathways of organic carbon downward transport by the oceanic biological carbon pump. *Frontiers in Marine Science*, *6*, 634. https://doi.org/10.3389/fmars.2019.00634

Nadaï, G., Nöthig, E.-M., Fortier, L., & Lalande, C. (2021). Early snowmelt and sea ice breakup enhance algal export in the Beaufort Sea. *Progress in Oceanography*, *190*, 102479. https://doi.org/10.1016/j.pocean.2020.102479

Nicol, S. (2003). Living krill, zooplankton and experimental investigations: A discourse on the role of krill and their experimental study in marine ecology. *Marine and Freshwater Behavior and Physiology*, *36*(4), 191–205. https://doi.org/10.1080/10236240310001614420

Nöthig, E.-M., Lalande, C., Fahl, K., Metfies, K., Salter, I., & Bauerfeind, E. (2020). Annual cycle of downward particle fluxes on each side of the Gakkel Ridge in the central Arctic Ocean. *Philosophical Transactions. Series A, Mathematical, Physical, and Engineering Sciences*, *378*(2181), 20190368. https://doi.org/10.1098/rsta.2019.0368

Onarheim, I. H., Eldevik, T., Smedsrud, L. H., & Stroeve, J. C. (2018). Seasonal and regional manifestation of Arctic sea ice loss. *Journal of Climate*, *31*(12), 4917–4932. https://doi.org/10.1175/jcli-d-17-0427.1

Onarheim, I. H., Smedsrud, L. H., Ingvaldsen, R. B., & Nilsen, F. (2014). Loss of sea ice during winter north of Svalbard. *Tellus*, *66*, 23933. https://doi.org/10.3402/tellusa.v66.23933

Oziel, L., Baudena, A., Ardyna, M., Massicotte, P., Randelhoff, A., Sallée, J.-B., et al. (2020). Faster Atlantic currents drive poleward expansion of temperate phytoplankton in the Arctic Ocean. *Nature Communications*, *11*(1), 1705. https://doi.org/10.1038/s41467-020-15485-5

Polyakov, I. V., Alkire, M. B., Bluhm, B. A., Brown, K. A., Carmack, E. C., Chierici, M., et al. (2020). Borealization of the Arctic Ocean in response to anomalous advection from sub-Arctic Seas. *Frontiers in Marine Science*, *7*, 491. https://doi.org/10.3389/fmars.2020.00491

Polyakov, I. V., Pnyushkov, A. V., Alkire, M. B., Ashik, I. M., Baumann, T. M., Carmack, E. C., et al. (2017). Greater role for Atlantic inflows on sea-ice loss in the Eurasian Basin of the Arctic Ocean. *Science*, *356*(6335), 285–291. https://doi.org/10.1126/science.aai8204

Popova, E. E., Yool, A., Aksenov, Y., & Coward, A. C. (2013). Role of advection in Arctic Ocean lower trophic dynamics: A modeling perspective: Advection in Arctic Ocean ecosystems. *Journal of Geophysical Research: Oceans*, *118*(3), 1571–1586. https://doi.org/10.1002/jgrc.20126

R Core Team. (2021). R: A language and environment for statistical computing. Retrieved from https://www.r-project.org/

Reigstad, M., Riser, C. W., Wassmann, P., & Ratkova, T. (2008). Vertical export of particulate organic carbon: Attenuation, composition and loss rates in the northern Barents Sea. *Deep Sea Research Part II: Topical Studies in Oceanography*, *55*(20–21), 2308–2319. https://doi.org/10.1016/j.dsr2.2008.05.007

Reigstad, M., & Wassmann, P. (2007). Does *Phaeocystis* spp. contribute significantly to vertical export of organic carbon? *Biogeochemistry*, *83*(1–3), 217–234. https://doi.org/10.1007/s10533-007-9093-3

Renner, A. H. H., Sundfjord, A., Janout, M. A., Ingvaldsen, R. B., Möller, A. B., Pickart, R. S., & Hernández, M. D. P. (2018). Variability and redistribution of heat in the Atlantic water boundary current north of Svalbard. *Journal of Geophysical Research: Oceans*, *123*(9), 6373–6391. https://doi.org/10.1029/2018jc013814

Riser, C. W., Reigstad, M., Wassmann, P., Arashkevich, E., & Falk-Petersen, S. (2007). Export or retention? Copepod abundance, fecal pellet production and vertical flux in the marginal ice zone through snapshots from the northern Barents Sea. *Polar Biology*, *30*(6), 719–730. https://doi.org/10.1007/s00300-006-0229-z

Riser, C. W., Wassmann, P., Reigstad, M., & Seuthe, L. (2008). Vertical flux regulation by zooplankton in the northern Barents Sea during Arctic spring. *Deep Sea Research Part II: Topical Studies in Oceanography*, *55*(20–21), 2320–2329. https://doi.org/10.1016/j.dsr2.2008.05.006

Roca-Martí, M., Puigcorbé, V., Iversen, M. H., van der Loeff, M. R., Klaas, C., Cheah, W., et al. (2017). High particulate organic carbon export during the decline of a vast diatom bloom in the Atlantic sector of the Southern Ocean. *Deep-Sea Research Part II*, *138*, 102–115. https://doi.org/10.1016/j.dsr2.2015.12.007

Roff, J. C., & Hopcroft, R. R. (1986). High precision microcomputer based measuring system for ecological research. *Canadian Journal of Fisheries and Aquatic Sciences*, *43*(10), 2044–2048. https://doi.org/10.1139/f86-251

Rynearson, T. A., Richardson, K., Lampitt, R. S., Sieracki, M. E., Poulton, A. J., Lyngsgaard, M. M., & Perry, M. J. (2013). Major contribution of diatom resting spores to vertical flux in the sub-polar North Atlantic. *Deep Sea Research Part I: Oceanographic Research Papers*, *82*, 60–71. https://doi.org/10.1016/j.dsr.2013.07.013

Sampei, M., Sasaki, H., Hattori, H., Forest, A., & Fortier, L. (2009). Significant contribution of passively sinking copepods to downward export flux in Arctic waters. *Limnology and Oceanography*, *54*(6), 1894–1900. https://doi.org/10.4319/lo.2009.54.6.1894

Smetacek, V. S. (1985). Role of sinking in diatom life-history cycles: Ecological, evolutionary, and geological significance. *Marine Biology*, *84*(3), 239–251. https://doi.org/10.1007/bf00392493

Søreide, J. E., Leu, E., Berge, J., Graeve, M., & Falk-Petersen, S. (2010). Timing of blooms, algal food quality and *Calanus glacialis* reproduction and growth in a changing Arctic. *Global Change Biology*, *12*. https://doi.org/10.1111/j.1365-2486.2010.02175.x

Stroeve, J., & Notz, D. (2018). Changing state of Arctic sea ice across all seasons. *Environmental Research Letters*, *13*(10), 103001. https://doi.org/10.1088/1748-9326/aade56

Sundfjord, A., Assmann, K. M., Lundesgaard, Ø., Renner, A. H. H., Lind, S., & Ingvaldsen, R. B. (2020). Suggested water mass definitions for the central and northern Barents Sea, and the adjacent Nansen Basin: The Nansen Legacy Report Series, (8). https://doi.org/10.7557/nlrs.5707

Sverdrup, H. U. (1953). On conditions for the vernal blooming of phytoplankton. *ICES Journal of Marine Science*, *18*(3), 287–295. https://doi.org/10.1093/icesjms/18.3.287

Tarling, G. A., Freer, J. J., Banas, N. S., Belcher, A., Blackwell, M., Castellani, C., et al. (2022). Can a key boreal *Calanus* copepod species now complete its life-cycle in the Arctic? Evidence and implications for Arctic food-webs. *Ambio*, *51*(2), 333–344. https://doi.org/10.1007/s13280-021-01667-y

Turner, J. T. (2015). Zooplankton fecal pellets, marine snow, phytodetritus, and the ocean's biological pump. *Progress in Oceanography*, *130*, 205–248. https://doi.org/10.1016/j.pocean.2014.08.005

Vernet, M., Ellingsen, I., Seuthe, L., Slagstad, D., Cape, M. R., & Matrai, P. A. (2019). Influence of phytoplankton advection on the productivity along the Atlantic water inflow to the Arctic Ocean. *Frontiers in Marine Science*, *6*. https://doi.org/10.3389/fmars.2019.00583

Vihtakari, M. (2020). PlotSvalbard: PlotSvalbard—Plot research data from Svalbard on maps. R package version 0.9.2. Retrieved from https://github.com/MikkoVihtakari/PlotSvalbard

von Bodungen, B., Antia, A., Bauerfeind, E., Haupt, O., Koeve, W., Machado, E., et al. (1995). Pelagic processes and vertical flux of particles: An overview of a long-term comparative study in the Norwegian Sea and Greenland Sea. *Geologische Rundschau*, *84*(1), 11–27. https://doi.org/10.1007/bf00192239

Wallace, M. I., Cottier, F. R., Brierley, A. S., & Tarling, G. A. (2013). Modeling the influence of copepod behavior on fecal pellet export at high latitudes. *Polar Biology*, *36*(4), 579–592. https://doi.org/10.1007/s00300-013-1287-7

Wassmann, P. (1998). Retention vs. export food chains: Processes controlling sinking loss from marine pelagic systems. In *Eutrophication in planktonic ecosystems: Food web dynamics and elemental cycling*, Eutrophication in Planktonic Ecosystems: Food Web Dynamics and Elemental Cycling (pp. 29–57). https://doi.org/10.1007/978-94-017-1493-8_3

Wassmann, P. (2001). Vernal export and retention of biogenic matter in the north-eastern North Atlantic and adjacent Arctic Ocean: The role of the Norwegian Atlantic current and topography. *Memoirs of National Institute of Polar Research. Special Issue*, *54*, 377–392.

Wassmann, P., Duarte, C. M., & Agusti, S. (2011). Footprints of climate change in the Arctic marine ecosystem. *Global Change*. https://doi.org/10.1111/j.1365-2486.2010.02311.x

Wassmann, P., Kosobokova, K. N., Slagstad, D., Drinkwater, K. F., Hopcroft, R. R., Moore, S. E., et al. (2015). The contiguous domains of Arctic Ocean advection: Trails of life and death. *Progress in Oceanography*, *139*, 42–65. https://doi.org/10.1016/j.pocean.2015.06.011

Wassmann, P., & Reigstad, M. (2011). Future Arctic Ocean seasonal ice zones and implications for pelagic-benthic coupling. *Oceanography*, *24*(3), 220–231. https://doi.org/10.5670/oceanog.2011.74

Wassmann, P., Slagstad, D., & Ellingsen, I. (2010). Primary production and climatic variability in the European sector of the Arctic Ocean prior to 2007: Preliminary results. *Polar Biology*, *33*(12), 1641–1650. https://doi.org/10.1007/s00300-010-0839-3

Wassmann, P., Slagstad, D., & Ellingsen, I. H. (2019). Advection of mesozooplankton into the northern Svalbard shelf region. *Frontiers in Marine Science*, *6*, 304. https://doi.org/10.3389/fmars.2019.00458

Wiedmann, I., Ershova, E., Bluhm, B. A., Nöthig, E.-M., Gradinger, R. R., Kosobokova, K., & Boetius, A. (2020). What feeds the Benthos in the Arctic Basins? Assembling a carbon budget for the deep Arctic Ocean. *Frontiers in Marine Science*, *7*, 224. https://doi.org/10.3389/fmars.2020.00224

Wolf, C., Iversen, M., Klaas, C., & Metfies, K. (2016). Limited sinking of *Phaeocystis* during a 12 days sediment trap study. *Molecular Ecology*, *25*(14), 3428–3435. https://doi.org/10.1111/mec.13697

Zhukova, N. G., Nesterova, V. N., Prokopchuk, I. P., & Rudneva, G. B. (2009). Winter distribution of euphausiids (Euphausiacea) in the Barents Sea (2000–2005). *Deep Sea Research Part II: Topical Studies in Oceanography*, *56*(21–22), 1959–1967. https://doi.org/10.1016/j.dsr2.2008.11.007